Layer-selective functionalisation in mesoporous double layer via iniferter initiated polymerisation for nanoscale step gradient formation

Mathias Stanzel[a], Ulrike Kunz[b], and Annette Andrieu-Brunsen[a,*]

[a]*Ernst-Berl Institut für Technische und Makromolekulare Chemie, Technische Universität Darmstadt, Alarich-Weiss-Strasse 8, D-64287 Darmstadt, Germany*
[b]*Department of Materials and Earth Sciences, Physical Metallurgy Group, Technische Universität Darmstadt, Alarich-Weiss-Straße 2, 64287 Darmstadt, Germany*

*Corresponding author. Tel.: +49-6151-16-23742
E-mail address: annette.andrieu-brunsen@tu-darmstadt.de

Functionalisation of technological nanopores and investigation of their transport properties have attracted considerable interest from scientific as from technological point of view, among others due to their potential regarding molecular transport design. Asymmetric design of nanopore structure and functionalisation is expected to trigger increased and directed transport of ionic species. Based on this motivation, we demonstrate a layer-selective polymer functionalisation in a mesoporous double layer thin film to generate nanoscale step gradient architectures with asymmetric charge distribution by taking advantage of co-condensation and polymer modification techniques. Thereby, mesoporous silica and co-condensed mesoporous amino silica thin films are combined to double layered films with a film thickness of 300 – 400 nm in both sequential arrangements, respectively. Iniferter initiated polymerisation is used to selectively functionalise only the amino silica layer with polymers such as [2-(methacryloyloxy)ethyl]trimethylammonium chloride (METAC) in a grafting from approach. Investigation of the ionic pore accessibility of the mesoporous double layered films before and after layer-selective polymer functionalisation shows that the ionic permselectivity is dominated by the bottom layer when overcoming the electrostatic repulsion of the top layer.

Keywords: layer-selective functionalisation, asymmetric charge distribution, mesoporous separation layer, iniferter polymerisation, transport modulation

1. Introduction

Modulation and understanding the transport of mass and charge in nanoscale pores and channels has attracted reasonable interest in the field of biology, chemistry, and physics, based on the transport phenomena that arise in such nanoconfined environment, which can be quite different to larger microscale dimension[1-4]. Particular interest of such porous systems can be assigned to the field of nanofluidics, as artificial nanoscale pores and channels have made major progress in the last two decades emerging applications in the field of biosensing, molecular transport, separation, drug delivery, and catalysis[5-8]. Thereby, recent results show that a break in symmetry of nanoscale pores and channels can lead to directional or gated transport of mass and charge similar to the outstanding performance of biological pores and channels[9-11]. For example, side-selective transport or oil-water separation is obtained by asymmetric wettability design of porous materials and membranes[12-16]. Preferential transport direction in nanochannels is also observed as diode-like ionic current rectification (ICR) phenomena by applying asymmetric pore geometry[17, 18]. For example, Siwy et al. demonstrated enhanced ICR ratios in the case of a conical pore compared to cylindrical pores[19]. Likewise, regardless of the pore geometry, enhanced ICR ratios have been observed, when the pore surface exhibits an asymmetric surface charge pattern, which has been comprehensively studied in experiment along with simulations[20-27]. Implementing this asymmetric design, bio-inspired artificial single ion pumps have been realised[28-30]. For example, Jiang and co-workers achieved pH regulated ion pumping by selectively functionalising the tip ends of an hour shaped nanochannel with cooperative pH-responsive polyelectrolytes[31]. Furthermore, selectively functionalising the outer surface of nanoporous materials can result in transient capping of the nanopore entrance allowing controlled release of guest molecules trapped inside the pores[32-34] or gating/switching of ionic transport[35-39]. Thus, influential factors for asymmetric ion transport behaviour that can be built in nanoscale structures are: nanopore geometry, surface charge distribution, chemical composition, and wettability

on the channel wall, as has been summarised by Guo et al.[40]. However, to meet the requirements for selectively regulating ion transport for advanced applications would require enhanced control over surface functionalisation in such nanoscale pores and channels, as well as detailed understanding of ion transport behaviour in nanoscale confinement.

In this context, mesoporous silica thin films (MSTF) representing solid-state nanopores have been utilised as model systems to manipulate ionic transport upon functionalisation providing fundamental insights of transport properties at the nanoscale.

In general, organic functionalities can be placed in MSTF by either co-condensation of inorganic precursors containing organic functional groups, or by post modification of the silica surface. Different polymerisation techniques, such as dye sensitised polymerisation[41], ring opening metathesis polymerisation (ROMP)[42], reversible addition-fragmentation chain-transfer polymerisation (RAFT) as well as iniferter initiated polymerisation[43], and atom transfer radical polymerisation (ATRP)[35] have been applied to generate hybrid MSTF. Thereby, regulation of transport has been demonstrated using stimuli, such as pH, temperature or light[44, 45].

In particular, tuneable functional densities and thus tailored transport properties arising from hybrid MSTF have been reported for the living radical polymerisation methods RAFT and iniferter initiated polymerisations[46]. Recently, our research group demonstrated that iniferter initiated polymerisations do not only offer the ability of controlled polymer amount and thus controlled functional density in mesopores, but also allow to control polymer chain's architecture by generation of block-cooligomers[47]. Nonetheless, in terms of MSTF, scientific reports on polymerisation methods for preparation of hybrid materials are limited to single layer system. Multilayered MSTF have been mainly focusing on optical properties and have been demonstrated as promising materials in photonics, sensing, and photocatalytic processes[48-50]. Thereby, in mesoporous multilayer, MSTF are often combined with mesoporous titania to form photonic crystals[51, 52]. In previous works, our group investigated transport properties of mesoporous and mesostructured double layer silica thin films by applying functional structure determining templates to form step gradient architectures[53, 54]. Yet, only a few examples investigating transport properties of multilayered mesoporous system can be found in literature.

Here, we demonstrate a strategy for layer-selective polymer functionalisation in mesoporous silica double layer films using iniferter initiated polymerisation in a grafting from approach for the formation of nanoscale step gradient architectures with asymmetric charge distribution on the nanoscale. We take advantage of the well-known co-condensation and post modification techniques of MSTF by integration of an amino group comprising precursor into one layer of a double layer MSTF, followed by selective binding of the iniferter to polymerise the positively charged monomer METAC layer-selectively. Thereby, we evaluate the functionalisation with respect to layer selectivity using IR spectroscopy, charged dye adsorption, as well as ellipsometry. Ionic pore accessibility of the functionalised double layer is investigated by applying cyclic voltammetry and discussed with respect to the layer arrangement. Thereby, we demonstrate that the ionic pore accessibility is dominated by the bottom layer that can overcome local electrostatic repulsion.

2. Experimental

2.1. Chemicals

All materials and solvents were purchased from Sigma-Aldrich, Acros Organics, and VWR and used as received unless stated otherwise. Microscope slides (VWR, glass, cut edges) were cleaned ethanol and dried under ambient conditions. Silicon wafers (Si-Mat, Kaufering, Germany, 100 mm diameter, 525 ± 25 µm thickness, type P/Bor, <100> orientation, CZ growth method, 2–5 W resistivity, polished on 1 side) and indium tin oxide (ITO, Delta Technologies, Ltd., Loveland, CO, USA, polished float glass, 150 x 150 x 1.1 mm, SiO_2 passivated/Indium Tin Oxide coated one surface, RS = 4–8 ohms, cut edges) were cut to desired size using a diamond cutter, cleaned using technical grade ethanol, and dried under ambient conditions prior to dip coating of mesoporous films.

2.2. Preparation of mesoporous double layer

Mesoporous thin films were prepared as previously described[55] via sol-gel chemistry using tetraethoxysilane (TEOS) and (3-aminopropyl)triethoxysilane (APTES) as inorganic precursors and an amphiphilic triblock copolymer, Pluronic® F127, as structure directing template that undergoes micellisation upon solvent evaporation resulting in formation of a porous inorganic network. The molar ratios of the compounds in the precursor solution used for dip coating were 1-x TEOS / x APTES / 0.0075 F127 / 40 EtOH / 10 H_20 / 0.28 HCl with x = 0 for silica thin films and x = 0.2 for amino silica thin films resulting in 6-10 nm mesopores. The precursor solutions were prepared at room temperature and stirred overnight prior the deposition on glass, silicon wafers and ITO covered glass applying the evaporation induced self-assembly (EISA)[56]. The films were dip coated at a withdrawal speed of 2 mm s^{-1} at 23 °C and 50% relative humidity. After deposition, the films were kept at 23 °C and 50% relative humidity for 1 h. The first film was then stabilised by a temperature treatment at 60 °C and 130 °C for 1 h respectively. The mesostructured bottom

layer was then covered with a second silica film via dip coating using the above mentioned conditions and stored at 23 °C and 50% relative humidity for 1 h. Finally, the mesoporous double layer was obtained, after template removal that was performed by extracting the mesoporous double layer in acidic ethanol (0.01 M HCl) for 3 days after consecutive temperature treatments at 60 °C, 130 °C for 1 h respectively and at 200 °C for 2 h.

2.3. Surface grafting of 4-(N,N-Diethyldithiocarbamoylmethyl)benzoic acid (BDC)

Surface grafting of BDC was performed under inert conditions and water was removed from all glass ware by heating under high vaccuum. A solution of 60 mg BDC (212 µmol, 1 eq) in 60 mL anhydrous DMF was prepared. Then, 46.7 µL *N,N*-Diisopropylethylamine (DIPEA, 275 µmol, 1.3 eq) and 104.6 mg 1-[Bis(dimethylamino)methylene]-1H-1,2,3-triazolo[4,5-b] pyridinium 3-oxide hexafluorophosphate (HATU, 275 µmol, 1.3 eq) were added and the solution stirred at room temperature for 15 minutes. The mesoporous double layer were immersed in the solution at room temperature overnight. Afterwards, the samples were intensively rinsed with DMF and ethanol to wash unbound BDC.

2.4. Iniferter initiated polymerisation of METAC

Polymer functionalisation was performed with BDC functionalised samples. Therefore, an aqueous 1 M solution of METAC was prepared and purged with nitrogen for 15 minutes. Then, the mesoporous double layer films were placed in the monomer solution and irradiated with UV light at a wavelength of 365 nm for 1 h. After polymerisation, the samples were extracted in deionised water for 1 h to remove unreacted monomer.

2.5. Attenuated Total Reflection Fourier Transform Infrared Spectroscopy (ATR-FTIR)

Infrared spectra of the prepared mesoporous films on glass substrates were recorded using a Perkin Elmer Instrument Spectrum One FT-IR Spectrometer equipped with a Universal ATR Polarisation Accessory (Waltham, MA, USA). All spectra were normalised to the stretching vibration of free silanol groups at ~905 cm^{-1}. The spectra were recorded using the Spectrum Software (Version 10.5.4.738, PerkinElmer, Inc. Waltham, MA, USA, 2016) between 4000 and 650 cm^{-1} with a resolution of 4 cm^{-1}. A background and a baseline correction was automatically performed. Additional bands of the glass substrate are visible in the FTIR spectra: Mesoporous film signals are partially superimposed by signals originating from the glass substrate in the region of 830 - 1250 cm^{-1} depending on the penetration depth of the ATR-IR evanescent waves. Nevertheless, due to the comparable film thickness, IR-spectra of different films can be compared. All further data processing was performed in OriginPro9 (ADDITIVE Soft- und Hardware für Technik und Wissenschaft GmbH, Friedrichsdorf, Germany, 2012).

2.6. Scanning Electron Microscopy (SEM)

SEM micrographs were obtained using a Philips XL30 FEG scanning electron microscope equipped with a tungsten cathode and a back scattered electron yttrium aluminium garnet (BSE YAG) detector with an accelerating voltage of 15–25 kV, a 30 µm aperture, and a spot size of 3–4. The samples were sputter-coated with a 7 nm coating of Pt/Pd. The digital micrographs were recorded over a range of magnifications at a working distance of 11 mm using an SE2 detector.

2.7. Transmission Electron Microscopy (TEM)

TEM micrographs were recorded using a Philips FEI CM-20 transmission electron microscope (Philips, Netherlands) equipped with a LaB_6 cathode and Olympus CCD camera, and with a maximum resolution of 2.3 Å operating at an accelerating voltage of 200 kV. Samples were prepared by scratching the mesoporous films and dispersion in filtered ethanol. After 5 min of sonication, scratched mesoporous films were drop cast onto 3.05 mm Cu grids (mesh size 200) with a Lacey carbon film (Plano GmbH, article number S166-2). The samples were dried under ambient conditions. For ultrathin sectioning, mesoporous double layer films were transferred on PET membrane discs (OxyDisc®, 13 mm diameter, Oxyphen, Germany) following the procedure of Lin et al.[57], embedded in Araldit© (polymerisation at 60 °C for 10 h) and cut in 70 nm sections using an ultramicrotome (Ultracut E, Reichert-Jung, Micro Star diamond knife).

2.8. Fluorescence imaging

Fluorescence images were recorded using a Fusion FX7 Edge imaging system (Vilber Lourmat, Germany).

2.9. Ellipsometry

The film thicknesses and refractive indices of mesoporous single- and double layer films deposited on silicon wafer substrates are determined using a Nanofilm EP3 imaging ellipsometer. By keeping the relative humidity constant at

15% relative humidity (humidity control: ACEflow, Solgelway), the one-zone angle of incidence (AOI) variation measurements are performed between AOIs of 38 ° and 68 ° in 2 ° steps using a laser wavelength of 658 nm. Film thicknesses and refractive indices are calculated using the measured ellipsometric angles Δ and Ψ with the software EP4 Model supplied with the instrument. The silicon oxide layer thickness of the substrate is kept constant at 4 nm. Layer thicknesses are fitted allowing an iteration between 100 and 200 nm for silica layers and iteration between 150 and 250 nm for amino silica layers respectively. The refractive indices are simultaneously fitted by iteration between the values 1.0 and 1.5. All films are measured on three spots along the direction of dip coating. Applying the Bruggeman effective medium approximation (BEMA), porosities and pore filling fractions are calculated with the refractive indices determined.

2.10. Cyclic voltammetry

The ionic pore accessibility of the mesoporous materials was investigated via cyclic voltammetry (CV) using $[Fe(CN)_6]^{3-/4-}$ and $[Ru(NH_3)_6]^{2+/3+}$ as charged, redox-active probe molecules. Measurements were recorded using a Metrohm Autolab PGSTAT302N potentiostat. Mesoporous films prepared on ITO coated glass substrates (Delta Technologies, Ltd., Loveland, CO, USA, polished float glass, 150 x 150 x 1.1 mm, SiO_2 passivated/Indium Tin Oxide coated one surface, RS = 4–8 ohms, cut edges) were characterised using a 1 mM solution of either the positively- or negatively charged probe molecule in a 100 mM KCl electrolyte solution. The pH-dependent permselectivity was investigated by adjusting the solution pH between 2 and 10 by the addition of either concentrated aqueous NaOH or HCl to the probe molecule containing buffer solutions. The pH was determined using a pH-meter (pH110, VWR). An Ag/AgCl reference electrode (BASi RE-6) and graphite counter electrode was used in the sample cell. The measured working electrode area was 0.21 cm^2. Pore accessibility for each pH was measured using a scan rate sequence of 200, 100, 25, 300, 1000, and 200 mV s^{-1}, with each scan rate being cycled three times. Quality control of the cyclic voltammograms was performed by ensuring comparability of the first and last scan rate, as well as between each scan of one rate. In addition, the first pH applied is re-measured for all scan rates ensuring reversible switching of charge and thus ionic pore accessibility.

3. Results and discussion

3.1. Structural characterisation of mesoporous thin films

The mesoporous films were prepared via well-established sol-gel chemistry and EISA[56] using TEOS and APTES as precursors and the amphiphilic triblock copolymer, Pluronic® F127, as structure directing template, as described in previous studies[55]. Thin multilayer layer films were deposited on glass, ITO coated glass, and silicon wafers via dip coating such that both individual layers, the bottom one as well as the top one are accessible for characterisation as depicted in Figure 1. MSTF with 160-190 nm thickness, ~40 vol% porosity, and mesoporous amino silica thin films with 230-240 nm film thickness and ~25-30 vol% porosity are obtained as determined from ellipsometry measurements (Table S1-S2). Both layers present ordered mesopore arrays with mesopore diameters in a range of 6-10 nm as expected from manifold previous studies[43, 47, 58, 59] and as analysed by TEM micrographs shown in Figure 1c, d. The resulting double layered mesoporous film architecture is well observed in SEM cross sectional measurement depicted in Figure 1e.

3.2. Layer-selective polymer functionalisation

Layer selective polymer functionalisation was achieved following a controlled iniferter initiated polymerisation approach which is schematically presented in Figure 1a. The photoiniferter BDC was synthesised according to a published protocol[60] and covalently bound to the surface amino groups of the amino silica layer via HATU coupling under formation of an amide (Figure S2 and S3). Investigation of chemical functionality of the mesoporous layers using ATR-IR spectroscopy shows layer-selective functionalisation of BDC exclusively on mesoporous amino silica. As the selective binding of BDC to amine groups determines subsequent local functionalisation, a careful extraction of unbound BDC has to be performed before polymerisation. Polymerisation of the monomer METAC was carried out in aqueous solution by applying UV light at a wavelength of 365 nm.

In order to investigate the chemical functionality of each individual layer as well as the double layer films through polymerisation of METAC, ATR-IR spectroscopy measurements have been performed before and after modification. Ideally, chemical modification as the result of

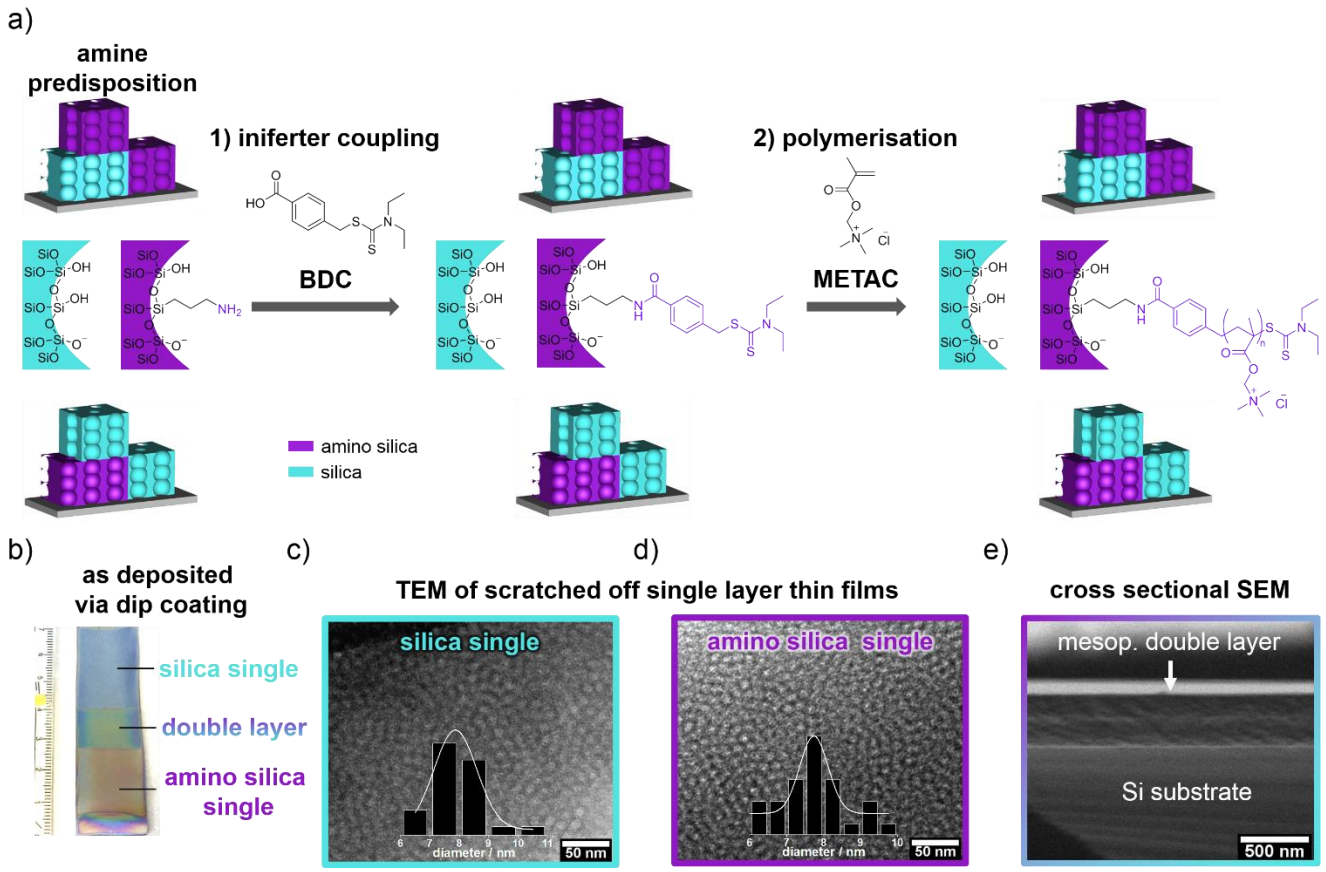

Fig. 1. Schematic representation of layer-selective functionalisation of mesoporous double layer architectures following an UV induced iniferter initiated polymerisation approach (a). Representative image of MSTF deposited on silicon wafer whereas both single layers and the double layer are present (b). TEM micrographs of MSTF (c) and mesoporous amino silica thin film (d), scale bar: 50 nm. SEM micrograph of a mesoporous double layer film cross section after polymerisation (e), scale bar: 500 nm.

iniferter-initiated METAC polymerisation is limited to the amino silica layer, as only these contain the covalently grafted initiator BDC. Comparing the ATR-IR spectra shown in Figure 2, all spectra display typical bands for mesoporous silica in the range of 650 and 1280 cm^{-1} indicating the presence of Si-O-Si (~1050 cm^{-1}) as well as Si-OH (~905 cm^{-1}) bands as discussed in previous studies[55, 61, 62]. The successful METAC polymerisation is validated based on the C=O vibrational band at 1725 cm^{-1} corresponding to the acrylate group of PMETAC. This C=O vibrational band originating from PMETAC functionalisation is observed for BDC functionalised amino silica single layers as well as in the double layer films after polymerisation (Figure 2, red curves) independently of the layer arrangement (BDC containing amino silica layer on top or at the bottom of a double layer film). This PMETAC C=O band at 1725 cm^{-1} is not observed in the ATR-IR spectra of the silica single layer indicating that these have not been functionalised with BDC and consequently do not contain grafted PMETAC as well as no physically adsorbed polymer. As mentioned above, layer-selective polymer functionalisation using grafting from requires a selective and locally confined binding of the iniferter for layer-selective polymer placement in mesoporous double layer films. The successful layer-selective functionalisation is achieved due to low unspecific adsorption of BDC, suitable MW of METAC allowing successful extraction of non-covalently bound species.

As the presence of the PMETAC C=O band in the ATR-IR spectra indicates a successful layer-selective polymerisation of METAC in the amino silica layers and thus nanoscale step gradient formation, further characterisation on layer selectivity has been conducted. Independently of pH, the PMETAC functionalised layer exhibit positively charged mesopores in consequence of the permanent positive charge of PMETAC. On the contrary, the mesoporous silica layers can be negatively or neutrally charged depending on the protonation state of surface silanol groups and thus depending on pH. For visualisation, mesoporous single layers as well as double layer, which were deposited on glass substrates, as demonstrated in Figure 1b, were immersed in aqueous fluorescein and rhodamine B

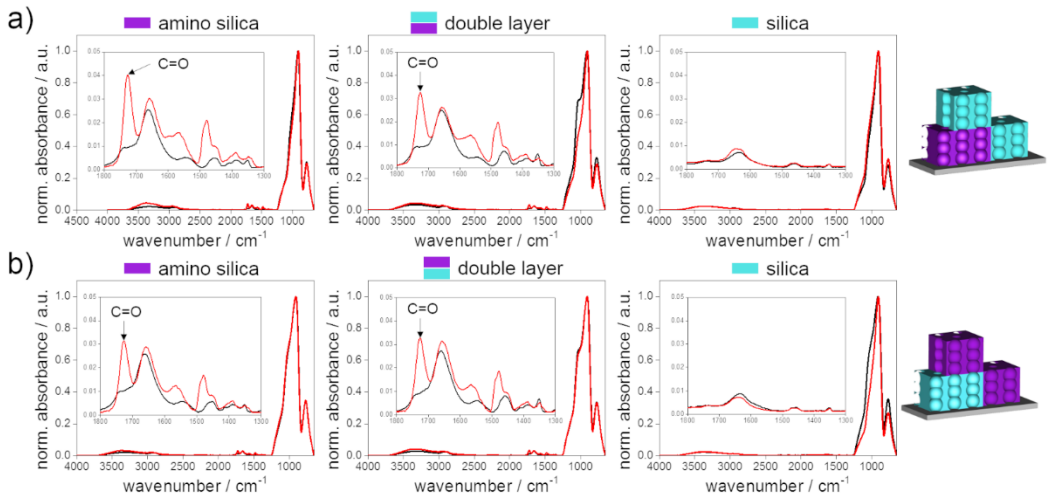

Fig. 2. ATR-IR spectra before (black curves) and after polymer modification (red curves) for single layer films and the double layer film with following sequence: silica layer at bottom - amino silica layer at top (a). ATR-IR spectra before (black curves) and after polymer modification (red curves) for single layer films and the double layer film with following sequence: amino silica layer at bottom - silica layer at top (b). For comparison, all spectra are normalised to the stretching vibration of free silanol groups at ~905 cm^{-1}.

solution at pH ~5, followed by analysis via fluorescence imaging. Charge-dependent dye adsorption is expected, as fluorescein carries a negative charge and the PMETAC functionalised amino silica layers exhibit a permanent positive charge, while rhodamine B carries a positive charge and the unmodified silica layers exhibit a negative charge. As shown in Figure 3a, the functionalised and thus positively charged PMETAC functionalised amino silica layers are coloured in magenta due to the physisorption of negatively charged fluorescein. The unmodified mesoporous layers are represented by the cyan coloured regions due to physisorption of positively charged rhodamine B into the negatively charged mesoporous silica. Note that the colour code matches rather the cartoons than the natural emission colour of the dyes. This charge selective dye adsorption further supports the successful layer-selective PMETAC functionalisation and thus step gradient formation, but as well indicates the potential relevance for transport control.

Following a published protocol from Lin et al.[57], double layer films were transferred from ITO coated glass substrates to PET membrane discs (OxyDisc®) allowing ultrathin sectioning of the samples and further analysis by TEM. Depicted in Figure 3b, the TEM micrograph shows the cross section of the mesoporous double layer film with the amino silica layer at the bottom and silica layer on top. A layer thickness of 206 ± 2 nm for the amino silica bottom layer, and a thickness of 137 ± 1 nm is obtained, which is in very good agreement to the thicknesses derived from ellipsometry measurements (Table S3-S4). Furthermore, the mesopore structure of the layers is very well observed indicating that no damage occurred upon the transfer from the solid substrate. Additional TEM micrographs can be found in Figure S4. Furthermore, EDX spectroscopy of the top-view of amino silica single layer as well as double layer films using SEM shows the presence of sulphur and nitrogen confirming successful iniferter coupling along with successful functionalization via polymerization (Figure S6).

Comparing the refractive indices obtained from ellipsometry measurements before and after applying the polymerisation conditions (Figure 3c-d, Table S1-S4), layer-selective functionalisation is further investigated. Thereby, an increase of the refractive index is expected in consequence of successful polymerisation, since PMETAC (assumption: n_{PMETAC} = 1.5 for organic molecules) replaces the volume of air (n_{air} = 1.0) in the porous material. Considering the single layers, MSTF show a slight decrease in refractive index indicating no functionalisation, whereas the mesoporous amino silica show an increased refractive index due to successful polymerisation of METAC. Pore filling of mesoporous amino silica single layer of 35-56 vol% is calculated by applying the BEMA and refractive indices before and after functionalisation. These observations are in agreement with the respective layers of the mesoporous double layer film, where the mesoporous silica layer is present as bottom layer and mesoporous amino silica layer on top (Figure 3d), and a pore filling of 84 vol% of the amino silica layer is calculated. Comparing the respective layers of the mesoporous double layer film, where the mesoporous amino silica layer is present as bottom layer and mesoporous silica layer on top (Figure 3c), again, an increased refractive index of the amino silica layer with a pore filling of 59 vol% is observed upon polymer functionalisation. Although the mesoporous silica bottom layer as well shows an increase in refractive index with a

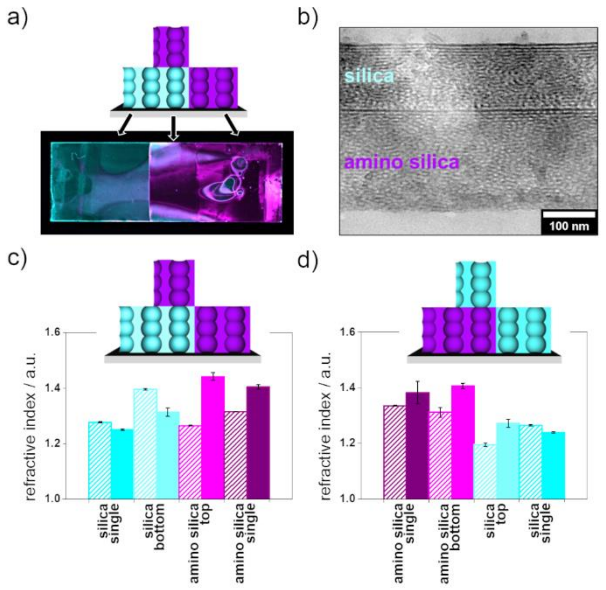

Fig. 3. Fluorescence image of single layers and double layer after subsequent incubation in aqueous fluorescein and rhodamine B solutions marking positively charged layers in magenta which can be attributed to METAC functionalised layers and negatively charged layers in cyan corresponding to the unmodified silica layers. Substrate size: 76 x 26 mm (a). Note, that the colour code does not represent the natural emission colour of the dyes used, but rather match the colour code of the cartoons. TEM micrograph of the mesoporous double layer film cross section after applying the polymerisation conditions, scale bar: 100 nm (b). Refractive indices obtained from ellipsometric measurements before (dashed columns) and after applying the polymerisation conditions (filled columns) for mesoporous single layer films and double layer films of the sequence: silica layer at bottom - amino silica layer at top (c) and for the sequence: amino silica layer at bottom - silica layer at top (d).

theoretical pore filling of 27 vol%, the initial refractive index (before functionalisation), as well as the film thickness (Table S2), seem to be an artefact of the complex model and undervalued from the fit, when compared to the mesoporous silica single layer, which had been exposed to the same experimental conditions (same substrate) showing no increase in refractive index. In an additional dataset of refractive index changes with lower polymer amount (pore filling 25 – 34 vol%) provided in the Supporting Information (Figure S1), this artefact is not observed, but again an increase of refractive index of mesoporous amino silica layers after polymerisation is observed in single and double layer arrangements. Thus, layer-selective functionalisation is further confirmed by ellipsometry measurements and high pore filling seems to result in difficulties fitting the obtained two layer films with strong refractive index step gradient.

3.3. Correlation to ionic permselectivity of mesoporous thin films

The ionic pore accessibility of the differently and pH-responsively charged mesoporous double layers deposited on conductive ITO coated glass substrates is characterised by cyclic voltammetry using the redox-active probe molecules $[Ru(NH_3)_6]^{2+/3+}$ and $[Fe(CN)_6]^{3-/4-}$, which result in a detected current at their redox potential after diffusing through the mesoporous film reaching the below ITO electrode. Measurements were performed at pH 2 and pH 10 for investigation of pH dependent negative charge of silica, which results from the deprotonation of silanol groups present on the pore wall surface at basic conditions. For the initial and hence unmodified double layers shown in Figure 4a, the expected pH-dependent ionic permselectivity is observed. At pH 2, $[Fe(CN)_6]^{3-/4-}$ is able to pass through the mesoporous film generating a current at the electrode upon oxidation and reduction. Thereby, no current density is detected for $[Ru(NH_3)_6]^{2+/3+}$, which can be ascribed to electrostatic repulsion and thus $[Ru(NH_3)_6]^{2+/3+}$ exclusion by the positively charged amine groups present in the amino silica layer. At pH 10, the negative charge of deprotonated silanol groups in both layers dominate the ionic mesopore accessibility. At this basic pH, $[Fe(CN)_6]^{3-/4-}$ is electrostatically excluded from the mesopores and no relevant current density is detected at the corresponding oxidation and reduction potential. Contrary to this, $[Ru(NH_3)_6]^{2+/3+}$ shows higher peak current densities as compared to an unmodified ITO electrode for both double layers, along with a peak broadening indicating a

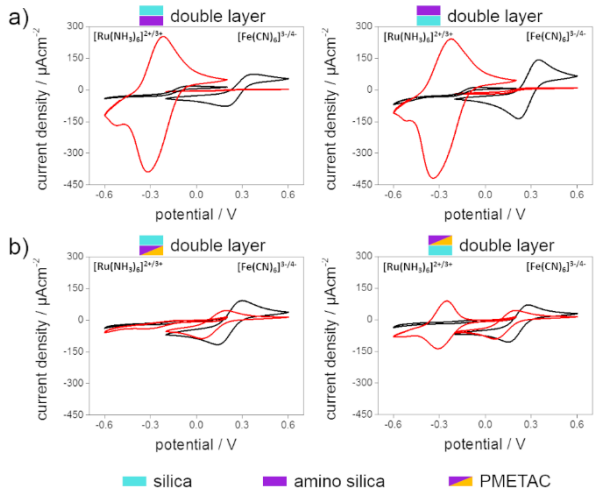

Fig. 4. Cyclic voltammograms of the mesoporous double layers using the redox active probe molecules $[Ru(NH_3)_6]^{2+/3+}$ and $[Fe(CN)_6]^{3-/4-}$ at concentration of 1 mM respectively in 100 mM KCl supporting electrolyte solution at pH 2 (black curves) and pH 10 (red curves) before (a) and after METAC functionalisation (b). Scan rate: 100 mV s^{-1}.

preconcentration of the probe molecule in the mesoporous film. Here, the peak current densities are 1.7 - 1.8 times higher as compared to an unmodified ITO electrodes (Figure S5). Considering the ionic pore accessibility of the double layer films after modification of the amino silica layer with PMETAC (Figure 4b), significant influence of the PMETAC functionalisation, but as well of the layer arrangement are observed, especially for the positively charged probe molecule $[Ru(NH_3)_6]^{2+/3+}$ (Figure 4b). At pH 2 (Figure 4b-c, black), where the silica layer is neutral in consequence of protonated silanol groups and the PMETAC functionalised amino silica layer positively charged, similar transport properties with respect to $[Fe(CN)_6]^{3-/4-}$ compared to before functionalisation are observed for both layer arrangements into a double layer film. Only a slightly reduced peak current density is detected compared to before functionalisation, which might arise due to steric hindrance upon functionalisation with PMETAC for both double layer arrangements. Under the same conditions, $[Ru(NH_3)_6]^{2+/3+}$ is not able to reach the ITO electrode underneath the mesoporous double layer film independently of the layer arrangement induced by the electrostatic repulsion of the PMETAC functionalised and thus positively charged layer. Differently to the unmodified double layers (Figure 4a) at basic conditions, an increase of peak current density is detected for $[Fe(CN)_6]^{3-/4-}$ at pH 10 after functionalisation with PMETAC for both layer arrangements indicating a weakening of the electrostatic repulsion of the negatively charged silanoate groups of the silica layer as result of incorporation of PMETAC in the amino silica layer, and thus positive charges. Interestingly, $[Fe(CN)_6]^{3-/4-}$ is even able to pass the negatively charged silica top layer (Figure 4b, left). In case the PMETAC functionalised layer is present as bottom layer, thus a step gradient from negatively charged top layer to positively charged bottom layer, no current density for $[Ru(NH_3)_6]^{2+/3+}$ is observed due to electrostatic repulsion of the positive charge induced by PMETAC functionalised amino silica bottom layer. A different result is obtained for the double layer with inverted layer arrangement containing the PMETAC functionalised, and thus positively charged amino silica as top layer, hence a step gradient from positively charged top layer to negatively charged bottom layer. For this layer arrangement, a peak current density is detected at pH 10, as $[Ru(NH_3)_6]^{2+/3+}$ is able to overcome the positively charged top layer probably by electrostatic attraction of the negatively charged bottom layer. This is a very interesting observation: a reduced peak current density is detected as compared to the unmodified double layer, although the present film thicknesses are much higher than the Debye Screening length (DBL) in these films (DBL here around ~1 nm). This indicates that the electrostatic repulsion in such systems can be locally overcome and ionic pore accessibility is dominated by the bottom layer, which is not in direct contact with the solution. The mesoporous double layers and layer-selective functionalisation presented serve as model systems for future mesoporous architectures, whose complexity can be further enhanced by, for example, increasing the number of the incorporated layers, which can be precisely adjusted in film thickness and pore dimensions, or compartmentalisation with other functional units like metal nanoparticles, along with further polymer functionalisation.

Conclusions

In summary, we described a layer-selective functionalisation strategy of mesoporous double layered films resulting in charge step gradient formation at the nanoscale. Key elements to this achievement are consecutive layer deposition of mesoporous silica films and co-condensed mesoporous amino silica films, thus predisposition of one layer, followed by layer-selective and controlled iniferter initiated polymerisation. The way of depositing the respective layers allows investigation of single as well as double layered films upon functionalisation granting indirect proof of layer-selective functionalisation by concluding the collective results obtained from IR spectroscopy, ellipsometry, charged dye immobilisation experiment, and cyclic voltammetry. Furthermore, the pH dependent ionic pore accessibility of the mesoporous double layered films before and after PMETAC functionalisation is investigated using cyclic voltammetry. Thereby, the bottom layer revealed a dominant role overcoming local electrostatic repulsion, even it is not in direct contact with the solution. We consider these results will broaden the possibility of creating complex mesoporous multilayer architectures toward multifunctional interfaces for nanofluidics and separation.

Acknowledgements

The authors kindly acknowledge the financial support by the “Forum für interdisziplinäre Forschung” (FiF, 2018#06) of the TU Darmstadt and funding from the European Research Council (ERC) under the European Union’s Horizon 2020 research and innovation programme (grant agreement No 803758). We especially thank Prof. Dr. Markus Biesalski (Chemistry Department, TU-Darmstadt) for access to interface characterisation facilities.

Data availability

The raw/processed data required to reproduce these findings cannot be shared at this time due to technical or time limitations.

References

[1] C. Dekker, Solid-state nanopores, Nat Nanotechnol 2 (2007) 209-15. https://doi.org/10.1038/nnano.2007.27.

[2] R.B. Schoch, J. Han, P. Renaud, Transport phenomena in nanofluidics, Reviews of Modern Physics 80 (2008) 839-883. https://doi.org/10.1103/RevModPhys.80.839.

[3] S.W. Kowalczyk, T.R. Blosser, C. Dekker, Biomimetic nanopores: learning from and about nature, Trends Biotechnol 29 (2011) 607-14. https://doi.org/10.1016/j.tibtech.2011.07.006.

[4] S. Zhang, T. Hedtke, X. Zhou, M. Elimelech, J.-H. Kim, Environmental Applications of Engineered Materials with Nanoconfinement, ACS ES&T Engineering (2021). https://doi.org/10.1021/acsestengg.1c00007.

[5] L. Bocquet, E. Charlaix, Nanofluidics, from bulk to interfaces, Chem Soc Rev 39 (2010) 1073-95. https://doi.org/10.1039/b909366b.

[6] H. Daiguji, Ion transport in nanofluidic channels, Chem Soc Rev 39 (2010) 901-11. https://doi.org/10.1039/b820556f.

[7] D.G. Haywood, A. Saha-Shah, L.A. Baker, S.C. Jacobson, Fundamental studies of nanofluidics: nanopores, nanochannels, and nanopipets, Anal Chem 87 (2015) 172-87. https://doi.org/10.1021/ac504180h.

[8] L. Bocquet, Nanofluidics coming of age, Nat Mater 19 (2020) 254-256. https://doi.org/10.1038/s41563-020-0625-8.

[9] S.F. Buchsbaum, G. Nguyen, S. Howorka, Z.S. Siwy, DNA-modified polymer pores allow pH- and voltage-gated control of channel flux, J Am Chem Soc 136 (2014) 9902-5. https://doi.org/10.1021/ja505302q.

[10] Z. Zhang, L. Wen, L. Jiang, Bioinspired smart asymmetric nanochannel membranes, Chem Soc Rev 47 (2018) 322-356. https://doi.org/10.1039/c7cs00688h.

[11] Y.A. Perez Sirkin, M. Tagliazucchi, I. Szleifer, Transport in nanopores and nanochannels: some fundamental challenges and nature-inspired solutions, Materials Today Advances 5 (2020) 100047. https://doi.org/10.1016/j.mtadv.2019.100047.

[12] H. Zhou, H. Wang, H. Niu, T. Lin, Superphobicity/philicity Janus fabrics with switchable, spontaneous, directional transport ability to water and oil fluids, Sci Rep 3 (2013) 2964. https://doi.org/10.1038/srep02964.

[13] Z. Wang, X. Yang, Z. Cheng, Y. Liu, L. Shao, L. Jiang, Simply realizing “water diode” Janus membranes for multifunctional smart applications, Materials Horizons 4 (2017) 701-708. https://doi.org/10.1039/c7mh00216e.

[14] M.B. Wu, H.C. Yang, J.J. Wang, G.P. Wu, Z.K. Xu, Janus Membranes with Opposing Surface Wettability Enabling Oil-to-Water and Water-to-Oil Emulsification, ACS Appl Mater Interfaces 9 (2017) 5062-5066. https://doi.org/10.1021/acsami.7b00017.

[15] M. Nau, N. Herzog, J. Schmidt, T. Meckel, A. Andrieu‐Brunsen, M. Biesalski, Janus‐Type Hybrid Paper Membranes, Advanced Materials Interfaces 6 (2019) 1900892. https://doi.org/10.1002/admi.201900892.

[16] Ç.K. Söz, S. Trosien, M. Biesalski, Janus Interface Materials: A Critical Review and Comparative Study, ACS Materials Letters 2 (2020) 336-357. https://doi.org/10.1021/acsmaterialslett.9b00489.

[17] Z. Siwy, A. Fulinski, Fabrication of a synthetic nanopore ion pump, Phys Rev Lett 89 (2002) 198103. https://doi.org/10.1103/PhysRevLett.89.198103.

[18] Z.S. Siwy, Ion-Current Rectification in Nanopores and Nanotubes with Broken Symmetry, Advanced Functional Materials 16 (2006) 735-746. https://doi.org/10.1002/adfm.200500471.

[19] Z. Siwy, Y. Gu, H.A. Spohr, D. Baur, A. Wolf-Reber, R. Spohr, P. Apel, Y.E. Korchev, Rectification and voltage gating of ion currents in a nanofabricated pore, Europhys Lett 60 (2002) 349-355. https://doi.org/DOI 10.1209/epl/i2002-00271-3.

[20] H. Daiguji, Y. Oka, K. Shirono, Nanofluidic diode and bipolar transistor, Nano Lett 5 (2005) 2274-80. https://doi.org/10.1021/nl051646y.

[21] L.J. Cheng, L.J. Guo, Ionic current rectification, breakdown, and switching in heterogeneous oxide nanofluidic devices, ACS Nano 3 (2009) 575-84. https://doi.org/10.1021/nn8007542.

[22] R. Yan, W. Liang, R. Fan, P. Yang, Nanofluidic diodes based on nanotube heterojunctions, Nano

Lett 9 (2009) 3820-5. https://doi.org/10.1021/nl9020123.
[23] Z.S. Siwy, S. Howorka, Engineered voltage-responsive nanopores, Chem Soc Rev 39 (2010) 1115-32. https://doi.org/10.1039/b909105j.
[24] C.-Y. Li, F.-X. Ma, Z.-Q. Wu, H.-L. Gao, W.-T. Shao, K. Wang, X.-H. Xia, Solution-pH-Modulated Rectification of Ionic Current in Highly Ordered Nanochannel Arrays Patterned with Chemical Functional Groups at Designed Positions, Advanced Functional Materials 23 (2013) 3836-3844. https://doi.org/10.1002/adfm.201300315.
[25] C.-Y. Lin, J.-P. Hsu, L.-H. Yeh, Rectification of ionic current in nanopores functionalized with bipolar polyelectrolyte brushes, Sensors and Actuators B: Chemical 258 (2018) 1223-1229. https://doi.org/10.1016/j.snb.2017.11.172.
[26] E. Madai, M. Valisko, D. Boda, Application of a bipolar nanopore as a sensor: rectification as an additional device function, Phys Chem Chem Phys 21 (2019) 19772-19784. https://doi.org/10.1039/c9cp03821c.
[27] Z.Q. Wu, Z.Q. Li, Y. Wang, X.H. Xia, Regulating Ion Transport in a Nanochannel with Tandem and Parallel Structures via Concentration Polarization, J Phys Chem Lett 11 (2020) 524-529. https://doi.org/10.1021/acs.jpclett.9b03016.
[28] X. Wu, P. Ramiah Rajasekaran, C.R. Martin, An Alternating Current Electroosmotic Pump Based on Conical Nanopore Membranes, ACS Nano 10 (2016) 4637-43. https://doi.org/10.1021/acsnano.6b00939.
[29] Z. Zhang, P. Li, X.Y. Kong, G. Xie, Y. Qian, Z. Wang, Y. Tian, L. Wen, L. Jiang, Bioinspired Heterogeneous Ion Pump Membranes: Unidirectional Selective Pumping and Controllable Gating Properties Stemming from Asymmetric Ionic Group Distribution, J Am Chem Soc 140 (2018) 1083-1090. https://doi.org/10.1021/jacs.7b11472.
[30] K. Xiao, L. Chen, R. Chen, T. Heil, S.D.C. Lemus, F. Fan, L. Wen, L. Jiang, M. Antonietti, Artificial light-driven ion pump for photoelectric energy conversion, Nat Commun 10 (2019) 74. https://doi.org/10.1038/s41467-018-08029-5.
[31] H. Zhang, X. Hou, L. Zeng, F. Yang, L. Li, D. Yan, Y. Tian, L. Jiang, Bioinspired artificial single ion pump, J Am Chem Soc 135 (2013) 16102-10. https://doi.org/10.1021/ja4037669.
[32] A. Bernardos, E. Aznar, M.D. Marcos, R. Martinez-Manez, F. Sancenon, J. Soto, J.M. Barat, P. Amoros, Enzyme-responsive controlled release using mesoporous silica supports capped with lactose, Angew Chem Int Ed Engl 48 (2009) 5884-7. https://doi.org/10.1002/anie.200900880.
[33] C. Coll, L. Mondragon, R. Martinez-Manez, F. Sancenon, M.D. Marcos, J. Soto, P. Amoros, E. Perez-Paya, Enzyme-mediated controlled release systems by anchoring peptide sequences on mesoporous silica supports, Angew Chem Int Ed Engl 50 (2011) 2138-40. https://doi.org/10.1002/anie.201004133.
[34] D.X. Zhang, C. Yoshikawa, N.G. Welch, P. Pasic, H. Thissen, N.H. Voelcker, Spatially Controlled Surface Modification of Porous Silicon for Sustained Drug Delivery Applications, Sci Rep 9 (2019) 1367. https://doi.org/10.1038/s41598-018-37750-w.
[35] A. Brunsen, J. Cui, M. Ceolin, A. del Campo, G.J. Soler-Illia, O. Azzaroni, Light-activated gating and permselectivity in interfacial architectures combining "caged" polymer brushes and mesoporous thin films, Chem Commun (Camb) 48 (2012) 1422-4. https://doi.org/10.1039/c1cc14443j.
[36] J. Elbert, F. Krohm, C. Rüttiger, S. Kienle, H. Didzoleit, B.N. Balzer, T. Hugel, B. Stühn, M. Gallei, A. Brunsen, Polymer-Modified Mesoporous Silica Thin Films for Redox-Mediated Selective Membrane Gating, Advanced Functional Materials 24 (2014) 1591-1601. https://doi.org/10.1002/adfm.201302304.
[37] X. Lin, Q. Yang, F. Yan, B. Zhang, B. Su, Gated Molecular Transport in Highly Ordered Heterogeneous Nanochannel Array Electrode, ACS Appl Mater Interfaces 8 (2016) 33343-33349. https://doi.org/10.1021/acsami.6b13772.
[38] S. Schmidt, S. Alberti, P. Vana, G. Soler-Illia, O. Azzaroni, Thermosensitive Cation-Selective Mesochannels: PNIPAM-Capped Mesoporous Thin Films as Bioinspired Interfacial Architectures with Concerted Functions, Chemistry 23 (2017) 14500-14506. https://doi.org/10.1002/chem.201702368.
[39] Q. Yang, X. Lin, Y. Wang, B. Su, Nanochannels as molecular check valves, Nanoscale 9 (2017) 18523-18528. https://doi.org/10.1039/c7nr05924h.
[40] W. Guo, Y. Tian, L. Jiang, Asymmetric ion transport through ion-channel-mimetic solid-state nanopores, Acc Chem Res 46 (2013) 2834-46. https://doi.org/10.1021/ar400024p.
[41] N. Herzog, J. Kind, C. Hess, A. Andrieu-Brunsen, Surface plasmon & visible light for polymer functionalization of mesopores and manipulation of

ionic permselectivity, Chem Commun (Camb) 51 (2015) 11697-700. https://doi.org/10.1039/c5cc03507d.
[42] F. Krohm, J. Kind, R. Savka, M. Alcaraz Janßen, D. Herold, H. Plenio, C.M. Thiele, A. Andrieu-Brunsen, Photochromic spiropyran- and spirooxazine-homopolymers in mesoporous thin films by surface initiated ROMP, Journal of Materials Chemistry C 4 (2016) 4067-4076. https://doi.org/10.1039/c5tc04054j.
[43] L. Silies, H. Didzoleit, C. Hess, B. Stühn, A. Andrieu-Brunsen, Mesoporous Thin Films, Zwitterionic Monomers, and Iniferter-Initiated Polymerization: Polymerization in a Confined Space, Chemistry of Materials 27 (2015) 1971-1981. https://doi.org/10.1021/cm503748d.
[44] S. Alberti, G.J. Soler-Illia, O. Azzaroni, Gated supramolecular chemistry in hybrid mesoporous silica nanoarchitectures: controlled delivery and molecular transport in response to chemical, physical and biological stimuli, Chem Commun (Camb) 51 (2015) 6050-75. https://doi.org/10.1039/c4cc10414e.
[45] G.J. Soler-Illia, O. Azzaroni, Multifunctional hybrids by combining ordered mesoporous materials and macromolecular building blocks, Chem Soc Rev 40 (2011) 1107-50. https://doi.org/10.1039/c0cs00208a.
[46] A. Brunsen, A. Calvo, F.J. Williams, G.J. Soler-Illia, O. Azzaroni, Manipulation of molecular transport into mesoporous silica thin films by the infiltration of polyelectrolytes, Langmuir 27 (2011) 4328-33. https://doi.org/10.1021/la200501h.
[47] J.C. Tom, R. Brilmayer, J. Schmidt, A. Andrieu-Brunsen, Optimisation of Surface-Initiated Photoiniferter-Mediated Polymerisation under Confinement, and the Formation of Block Copolymers in Mesoporous Films, Polymers (Basel) 9 (2017). https://doi.org/10.3390/polym9100539.
[48] L.A. Villaescusa, A. Mihi, I. Rodriguez, A.E. Garcia-Bennett, H. Miguez, Growth of mesoporous materials within colloidal crystal films by spin-coating, J Phys Chem B 109 (2005) 19643-9. https://doi.org/10.1021/jp053511m.
[49] P.C. Angelomé, M.C. Fuertes, G.J.A.A. Soler-Illia, Multifunctional, Multilayer, Multiscale: Integrative Synthesis of Complex Macroporous and Mesoporous Thin Films with Spatial Separation of Porosity and Function, Advanced Materials 18 (2006) 2397-2402. https://doi.org/10.1002/adma.200600439.
[50] T. Brezesinski, M. Antonietti, B.M. Smarsly, Self-Assembled Metal Oxide Bilayer Films with “Single-Crystalline” Overlayer Mesopore Structure, Advanced Materials 19 (2007) 1074-1078. https://doi.org/10.1002/adma.200602867.
[51] M. Faustini, D.R. Ceratti, B. Louis, M. Boudot, P.A. Albouy, C. Boissiere, D. Grosso, Engineering functionality gradients by dip coating process in acceleration mode, ACS Appl Mater Interfaces 6 (2014) 17102-10. https://doi.org/10.1021/am504770x.
[52] M. Faustini, L. Nicole, C.d. Boissière, P. Innocenzi, C.m. Sanchez, D. Grosso, Hydrophobic, Antireflective, Self-Cleaning, and Antifogging Sol−Gel Coatings: An Example of Multifunctional Nanostructured Materials for Photovoltaic Cells, Chemistry of Materials 22 (2010) 4406-4413. https://doi.org/10.1021/cm100937e.
[53] N. Herzog, H. Hübner, C. Rüttiger, M. Gallei, A. Andrieu-Brunsen, Functional Metalloblock Copolymers for the Preparation and In Situ Functionalization of Porous Silica Films, Langmuir 36 (2020) 4015-4024. https://doi.org/10.1021/acs.langmuir.0c00245.
[54] J.C. Tom, C. Appel, A. Andrieu-Brunsen, Fabrication and in situ functionalisation of mesoporous silica films by the physical entrapment of functional and responsive block copolymer structuring agents, Soft Matter 15 (2019) 8077-8083. https://doi.org/10.1039/c9sm00872a.
[55] N. Herzog, R. Brilmayer, M. Stanzel, A. Kalyta, D. Spiehl, E. Dörsam, C. Hess, A. Andrieu-Brunsen, Gravure printing for mesoporous film preparation, RSC Advances 9 (2019) 23570-23578. https://doi.org/10.1039/c9ra04266k.
[56] C.J. Brinker, Y. Lu, A. Sellinger, H. Fan, Evaporation-Induced Self-Assembly: Nanostructures Made Easy, Adv Mater 11 (1999) 579-585.
[57] X. Lin, Q. Yang, L. Ding, B. Su, Ultrathin Silica Membranes with Highly Ordered and Perpendicular Nanochannels for Precise and Fast Molecular Separation, ACS Nano 9 (2015) 11266-77. https://doi.org/10.1021/acsnano.5b04887.
[58] A. Calvo, M. Joselevich, G.J.A.A. Soler-Illia, F.J. Williams, Chemical reactivity of amino-functionalized mesoporous silica thin films obtained by co-condensation and post-grafting routes, Microporous and Mesoporous Materials 121 (2009) 67-72. https://doi.org/10.1016/j.micromeso.2009.01.005.

[59] M.G. Bellino, S. Municoy, G.J.A.A. Soler-Illia, Enzymatic tandem systems engineered from mesoporous thin films: Synergy leading to efficient starch-electricity conversion, Materials Today Communications 7 (2016) 67-72. https://doi.org/10.1016/j.mtcomm.2016.04.002.
[60] T. Magoshi, H. Ziani-Cherif, S. Ohya, Y. Nakayama, T. Matsuda, Thermoresponsive Heparin Coating: Heparin Conjugated with Poly(N-isopropylacrylamide) at One Terminus, Langmuir 18 (2002) 4862-4872. https://doi.org/10.1021/la011408s.
[61] P. Innocenzi, Infrared spectroscopy of sol–gel derived silica-based films: a spectra-microstructure overview, Journal of Non-Crystalline Solids 316 (2003) 309-319.
[62] A. Calvo, P.C. Angelomé, V.M. Sánchez, D.A. Scherlis, F.J. Williams, G.J.A.A. Soler-Illia, Mesoporous Aminopropyl-Functionalized Hybrid Thin Films with Modulable Surface and Environment-Responsive Behavior, Chemistry of Materials 20 (2008) 4661-4668. https://doi.org/10.1021/cm800597k.